

Supplemental Material: Pattern generation by dissipative parametric instability

A. M. Perego^{1,2}, N. Tarasov^{1,3}, D. V. Churkin^{1,4,5}, S. K. Turitsyn^{1,4} and K. Staliunas^{2,6}

¹ Aston Institute of Photonic Technologies, Aston University, Birmingham B4 7ET, UK

² Departament de Física i Enginyeria Nuclear, Universitat Politècnica de Catalunya, E-08222, Barcelona, Spain

³ Institute of Computational Technologies SB RAS, Novosibirsk, 630090, Russia

⁴ Novosibirsk State University, Novosibirsk, 630090, Russia

⁵ Institute of Automation and Electrometry SB RAS, Novosibirsk, 630090, Russia

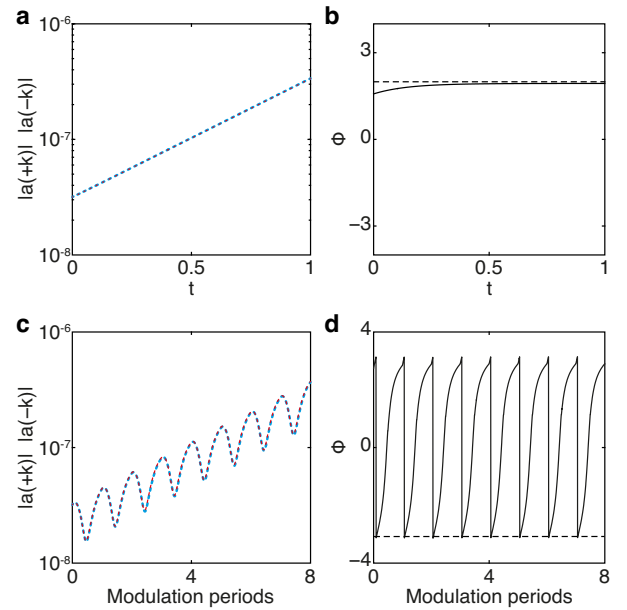
⁶ Institució Catalana de Recerca i Estudis Avançats, Passeig Lluís Companys 23, E-08010, Barcelona, Spain

In order to perform the numerical stability analysis of Eq. (1), we first calculated the homogeneous solution. Then we added a small complex perturbation to each spectral mode of the spectrum and integrated the CGLE for one modulation period T_f . To be more specific, a 4 by 4 transfer matrix M was obtained for each mode pair $+k$ and $-k$, whose first and second row entries are the real and imaginary parts of the modes $+k$ and $-k$ amplitudes after the evolution of real and imaginary perturbations to mode k . The third and fourth rows of M contain the real and imaginary parts of $+k$ and $-k$ mode amplitudes, respectively, after the evolution of real and imaginary perturbations of mode $-k$. The resulting modes' amplitudes were normalized to the initial perturbation's absolute value.

The diagonalization of matrix M provides a set of four eigenvalues $F(k)$ for modes $+k$ and $-k$: the so-called Floquet multipliers. A mode k is considered unstable when at least one of the absolute values of its eigenvalues is greater than 1. To visualize the instability spectrum, we plotted $\text{Max}(|F(k)|)$ – the maximal absolute value of the Floquet multipliers – for each mode. As the instability spectrum is symmetric, only the positive part the spectrum ($k > 0$) has been plotted.

The mechanism of dissipative parametric modulation instability differs from those of the classical Benjamin-Feir and Faraday instability due to its *antiphase* modulation dynamics depicted in Fig. 3(b) of the main article. Specifically, the amplitudes of modulation modes symmetrically located at $+k$ and $-k$, respectively, both grow on average over time. During this increase, however, their amplitudes are not equal at every instant point of evolution due to the action of the spectrally dependent losses. This feature clearly distinguishes the reported dissipative parametric instability from the BF and the Faraday ones.

In the case of Faraday instability, the growth process is synchronized with the external forcing. In the Benjamin-Feir case, since no periodic forcing is applied, the growth is due to the increase of the small perturbations during the evolution (see Supplemental Fig. 1). Hence, the synchronization with the external forcing is a common feature of both Faraday and dissipative parametric instability.



Supplemental FIG. 1. Growth process of the symmetrically (in wavenumber space) located maximally unstable modes $a(+k)$ and $a(-k)$ (blue and dashed red line) (a) and generalized phase (b) for the BF instability. The same for the Faraday instability: modes (c) and generalized phase (d). Dashed lines in (b) and (d) correspond to the optimum value of the generalized phase for synchronization with the homogeneous mode. For Faraday instability, the oscillatory growth process is synchronized with the external forcing. The parameters used are those considered in Fig. 1 of the main article.

We provide now a heuristic explanation of the growth of the unstable modes in the dissipative parametric instability of the CGLE, showing how, in presence of the alternating (zig-zag) damping, the coupling between modes can provide the energy necessary for the growth. Let us consider the CGLE (Eq. (1) of the main article). After perturbation of the homogeneous solution choosing the following *ansatz* for the field $A(t, x) = A_0 \exp(ic|A_0|^2 t) [1 + a_+ \exp(ikx) + a_- \exp(-ikx)]$; and linearization of CGLE with respect to the small perturbations, the evolution equation for the modulation mode $a_{+k}(t)$, reads:

$$\frac{\partial a_+}{\partial t} = \mu a_+ - bk^2 a_+ + idk^2 a_+ + ic(a_+ + a_-^*)A_0^2 - s(2a_+ + a_-^*)A_0^2. \quad (\text{SE } 1)$$

The (+) mode is coupled to the mode $a_{-k}^*(t)$:

$$\frac{\partial a_-^*}{\partial t} = \mu a_-^* - bk^2 a_-^* - idk^2 a_-^* - ic(a_+ + a_-^*)A_0^2 - s(2a_-^* + a_+)A_0^2. \quad (\text{SE } 2)$$

The solution of Supplemental Eqs. (1) and (2) can be sought in the form of exponentially decaying oscillations (Bogoliubov-De Gennes excitations): $a(t) = \exp(Dt) [a_1 \cos(\omega_B t) + a_2 \sin(\omega_B t)]$. The frequency of the oscillations ω_B and the damping rate D , are given by the imaginary and real part of the eigenvalue spectrum of the CGLE, respectively:

$$\lambda_{\pm} = -\mu - bk^2 \pm \sqrt{-d^2 k^4 - 2cdk^2 \mu/s + \mu^2}. \quad (\text{SE } 3)$$

In the limit $d^2 k^4 + 2cdk^2 \mu/s > \mu^2$, the frequency and the damping coefficient are, respectively:

$$\omega_B = \sqrt{d^2 k^4 + 2cdk^2 \mu/s - \mu^2} \quad (\text{SE } 4)$$

$$D = -\mu - bk^2 \quad (\text{SE } 5)$$

and the corresponding solutions of Supplemental Eqs. (1) and (2) read:

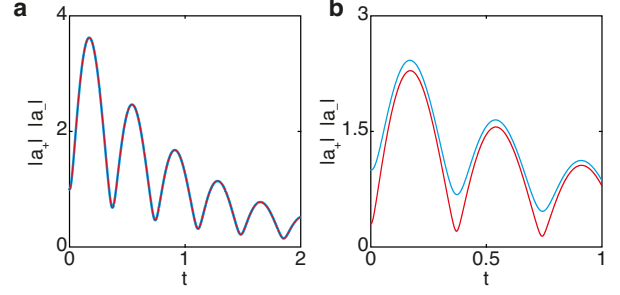
$$a_+(t) = \exp[(-\mu - bk^2)t] \{ \tilde{a}_+ \cos(\omega_B t) + [\tilde{a}_-^*/\omega_B (ic \mu/s - \mu) + \tilde{a}_+/\omega_B (idk^2 + ic \mu/s)] \sin(\omega_B t) \} \quad (\text{SE } 6)$$

$$\tilde{a}_-^*(t) = \exp[(-\mu - bk^2)t] \{ \tilde{a}_-^* \cos(\omega_B t) + [\tilde{a}_+/\omega_B (-ic \mu/s - \mu) + \tilde{a}_-^*/\omega_B (-idk^2 - ic \mu/s)] \sin(\omega_B t) \} \quad (\text{SE } 7)$$

with $a_+(0) = \tilde{a}_+$ and $a_-^*(0) = \tilde{a}_-^*$. We can obtain the temporal evolution for the mode $a_{-k}(t)$ by taking the complex conjugate of Supplemental Eq. (7):

$$a_-(t) = \exp[(-\mu - bk^2)t] \{ \tilde{a}_- \cos(\omega_B t) + [\tilde{a}_+^*/\omega_B (ic \mu/s - \mu) + \tilde{a}_-/\omega_B (idk^2 + ic \mu/s)] \sin(\omega_B t) \} \quad (\text{SE } 8)$$

where $\tilde{a}_- = a_-(0)$.



Supplemental FIG. 2. Temporal evolution of Bogoliubov-De Gennes modes for $k = \pm 100 \times 2\pi$ obtained evaluating Supplemental Eqs. (6) and (8) with the same parameters as in Fig. 3 of the main article. The excitations experience oscillatory behaviour with asymptotic decay of the amplitudes (blue and over-imposed dashed red line) (a) when the initial conditions are equal; in particular, we have chosen $\tilde{a}_+ = \tilde{a}_- = 1$. When one mode is damped, a rapid growth of its amplitude occurs, as shown in (b); in this case $\tilde{a}_+ = 1$ and $\tilde{a}_- = 0.3$. Alternating the damping of modes $\pm k$ with a temporal periodicity, which allows the successive growth of the damped mode, leads to the average growth of both sidebands, resulting in the dissipative parametric instability.

The amplitudes of the excitations exponentially decay asymptotically, oscillating at frequency ω_B as illustrated in Supplemental Fig. 2(a). However, when the initial amplitude of one mode, say a_- , is much lower than the amplitude of the other one, a_+ , then the amplitude of a_- grows due to the coupling, as depicted in Supplemental Fig. 2(b).

When the losses for modes a_- and a_+ are introduced in an alternating way and with a period large enough to allow for the growth of the damped mode – but not too large – to avoid the asymptotic decay, then an average growth of a_- and a_+ occurs.

The evolution described in terms of Supplemental Eqs. (6) and (8) is valid in the linear regime, when the quadratic terms in the mode amplitudes are negligible. In order to describe the nonlinear dynamics, numerical integration of the master Eq. (1) of the main paper is required. Nevertheless, the linear analysis presented above sheds light on how the instability develops before entering the nonlinear regime, where the sidebands amplitudes are no longer small and the saturation process takes place. In principle, the instability can develop as a result of periodically imposed losses only on one mode (say with wavenumber k) or on a spectral region (say $+\Delta k$), this kind of excitation could not lead to pattern formation – only to a frequency shift in the spectrum. In order to achieve pattern formation, the spectral zig-zag modulation configuration is required.

Motivated by the synchronization between the growing modes and the external forcing shown in Fig. 3(b) of the main article, we present here an analytical estimate of the wavenumber of the maximally growing mode of the dissipative parametric instability (dashed black line in Fig. 3(d)). This is done by imposing the parametric resonance condition to the dispersion relation of the dissipative Bogoliubov modes of the CGLE. This

condition assumes that the first excited mode has a wavenumber that is related, via the dispersion relation $\omega(k)$, to a temporal frequency equal to half of the forcing one. Starting from the instability spectrum of the CGLE, the dispersion relation is given by Supplemental Eq. (4). In the long wave limit, $2cdk^2\mu/s \gg d^2k^4$, Supplemental Eq. (4) simplifies to: $\omega_B = \sqrt{2cdk^2\mu/s - \mu^2}$, which allows straightforwardly to estimate, for $\mu \leq \pi/T_f$, the wavenumber of the first excited mode k_{inst} by imposing the parametric resonance condition:

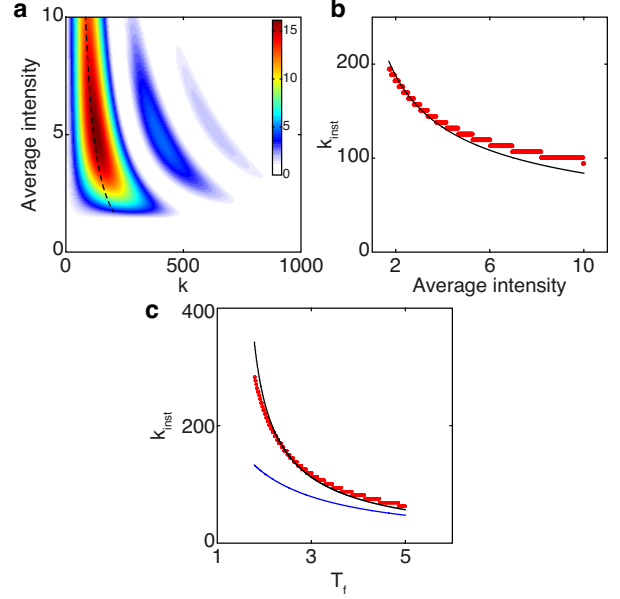
$$k_{\text{inst}} \approx \frac{(\pi/T_f)}{\sqrt{2cd\mu/s}}. \quad (\text{SE } 9)$$

Supplemental Eq. (9) is generic and gives the estimate of the first unstable mode for the parametric instabilities. In the presence of strongly detuned filters, the homogeneous field intensity $|A_0|^2$ is not exactly equal to the nominal value μ/s , since the strongly detuned filters can damp the homogeneous mode. However, we have checked that the minor damping of the homogeneous mode due to the detuned filters is not a necessary condition for the development of the dissipative parametric instability. In the absence of filters, selective and alternate damping of modes placed at $\pm k$ leads to their average growth. To plot the theoretical prediction (on Fig. 3(d)), we calculated k_{inst} from Supplemental Eq. (9), using the intensity numerically averaged over one modulation period, instead of μ/s . In Supplemental Fig. 3(c) this scaling is compared with the one that results from Supplemental Eq. (9) evaluated with the nominal value of μ/s .

We have also considered an instability map similar to the one shown in Fig. 3(d) of the main article, but obtained for fixed modulation period and varying μ . The instability map depicted in Supplemental Fig. 3(a) shows the unstable region as a function of the average intensity, which differs from the nominal value μ/s (Supplemental Fig. 3(b)) for the reasons mentioned above.

Another distinctive feature of the dissipative parametric instability is the scaling of the wavenumber of the most unstable mode with respect to the amplitude of the background wave. Our calculations at different wave amplitudes A_0 indicate that the maximally growing wavenumber decreases with field intensity (Supplemental Fig. 3), as can be expected for Faraday instability. This phenomenon contrasts with the well-known BF instability scaling in which the wavenumber of the maximally unstable mode always increases with the amplitude of the homogeneous field, in other words, with nonlinearity.

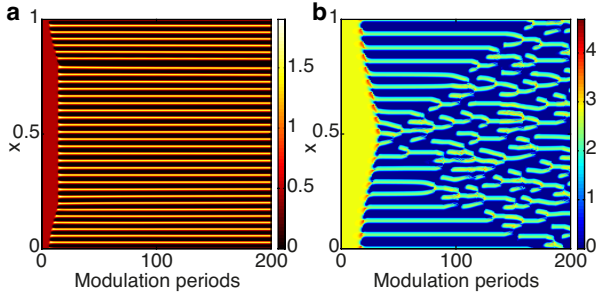
Despite its phenomenological origin Supplemental Eq. (9) provides a useful tool for a qualitative (or semi-quantitative) description of the dissipative parametric instability.



Supplemental FIG. 3. Instability map obtained varying μ from 0.5 to 2.142 and plotted in the wavenumber-average intensity space (a); the coloured regions correspond to instability; the remaining parameters are the same as in Fig. 3 of the main article. The scaling of the maximally unstable mode k_{inst} versus the field intensity (b): red points are the results of Floquet analysis, the black line is Supplemental Eq. (9) with μ/s substituted by the effective average intensity calculated numerically. In (c), the scaling of the maximally unstable mode versus T_f corresponds to Fig. 3(d) in the main article. The black line corresponds to Supplemental Eq. (9) using the average intensity, while the blue one is Supplemental Eq. (9) with the nominal value of the ratio μ/s .

In the main article, we have provided an example of a pattern formation initiated by the dissipative parametric modulation instability. Even though a detailed study of the pattern stability conditions in the asymptotic nonlinear regime is beyond the scope of this study, we provide here two examples of regular and irregular patterns showing their temporal evolution. In Supplemental Fig. 4(a), a regular periodic pattern is depicted corresponding to the parameters used in Fig. 3 of the main article. Supplemental Fig. 4(b) shows the possibility of irregular patterns where repeated processes of creation and annihilation of spatial structures occur. The irregular pattern has been generated by reducing the detuning of the filters while retaining the remaining parameters as in the case of regular patterns. Supplemental Figs. 4(a) and 4(b) both depict a set of frames showing the spatial distribution of field intensity taken at the end of each modulation period, right after the second filter. We call a pattern “stable” if its shape remains unchanged for used long simulation time. Note, that this consideration does not prove true stability, but it gives a good indication of a possible stability of such patterns. As further check we have verified that performing the simulations which lead to pattern formation like the ones in Figs. 3(f) and 4(c), also in presence of additive noise, the resulting patterns remain unchanged. Stable patterns form when the noisy background which develops between the

coherent structures is efficiently suppressed due to the combined action of nonlinear-dispersive spectral broadening and dissipative periodic filtering. If such suppression does not occur, then neighbour structures can grow between the already existing ones entering into competition with them with a related creation and annihilation process, as it is illustrated in Supplemental Fig. 4(b). The presence of diffusion helps the pattern stabilization.

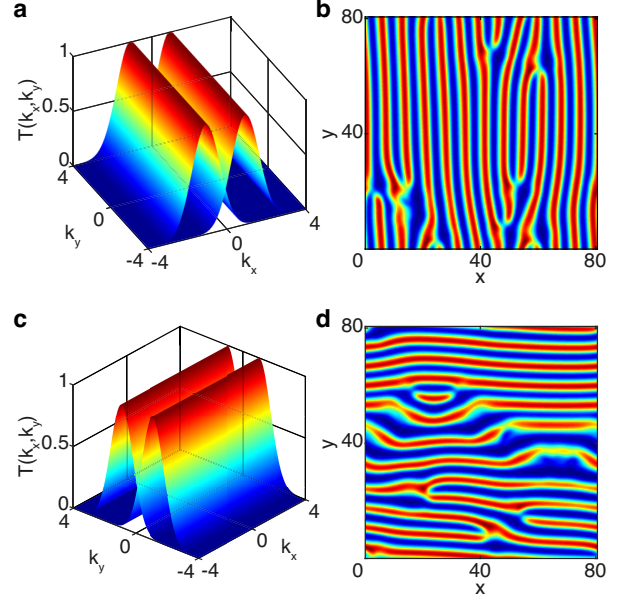


Supplemental FIG. 4. Temporal evolution of the one-dimensional patterns generated by the dissipative parametric instability. In (a), a stable pattern corresponding to the case of Fig. 3 of the main article is depicted; while in (b) the temporal dynamics of an unstable pattern shows continuous processes of creation and annihilation of coherent structures. Figure (b) has been obtained using $k_0 = 1570.8$, while keeping the remaining parameters as in (a).

Pattern formation through dissipative parametric instability in the two-dimensional system gives more freedom in the choice of the structure of the dissipative elements. Here we provide more details of the scheme illustrated in the main article and show them in Supplemental Figs. 5(a) and 5(b) where the dissipation function takes the form:

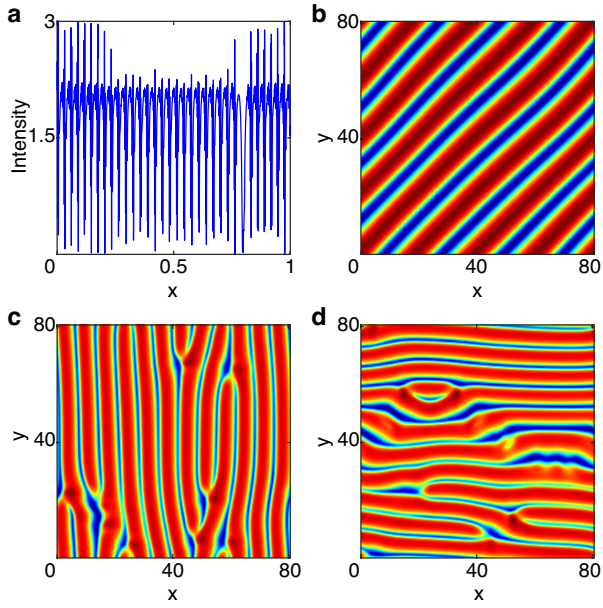
$$f_{1,2} = \exp[-(k_x \pm k_{0x})^2 / \sigma^2]. \quad (\text{SE } 10)$$

In contrast with the results presented in Fig. 4 of the main article, the patterns shown in Supplemental Fig. 5 are not tilted, because of the different shape of the dissipation in wavenumber space. A similar pattern, but with a spatial modulation along the orthogonal direction y , can be obtained by using the same dissipation function as in Supplemental Eq. (10), but replacing k_x with k_y and k_{0x} with k_{0y} (see Supplemental Figs. 5(c) and 5(d)).



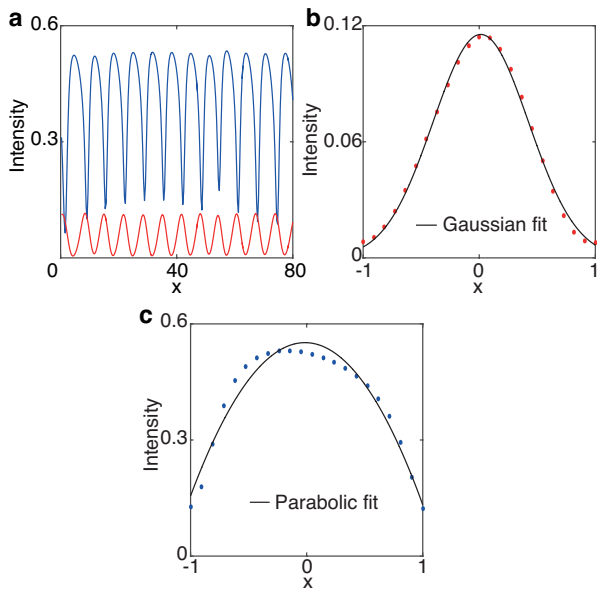
Supplemental FIG. 5. The two Gaussian transmission functions used to modulate the dissipation (a) and the corresponding 2-dimensional pattern created due to dissipative parametric instability (b) for $k_{0x} = 1$. A $\pi/2$ rotation in k -space of the transmission function (exchange of k_x with k_y and k_{0x} with k_{0y}) for $k_{0y} = 1$, leads to the generation of a pattern with a periodicity along the spatial direction y (d). The parameters used are as follows: $\mu = 0.2$, $d = 0.05$, $b = 0.001$, $c = 0.35$, $s = 0.3$, $T_f = 5\pi$, and $\sigma = 1$.

We finally provide a phenomenological characterization of the patterns temporal evolution and functional shape. Once the pattern has appeared through progressive increase of the modulation of the homogeneous field background, the individual coherent structures which form the pattern evolve dynamically and periodically during each modulation period. The evolution in normal diffraction, in presence of gain, resembles the formation of similaritons in fiber amplifiers and leads to a considerable broadening associated with a modification of the original Gaussian shape into an almost parabolic one. The patterns shapes at the end of the nonlinear evolution just before the filter action are reported in Supplemental Fig. 6.



Supplemental FIG. 6. In (a) the 1-D pattern just before the filter action is depicted: the structures exhibit a clear broadening towards parabolic shape, while high frequency noise spikes are clearly visible between neighbour structures. In 2D we have the same broadening effect towards parabolic shape: (b), (c) and (d) are the corresponding intensity profiles before filter action for Fig. 4(c), Supplemental Figs. 5(b) and 5(d).

We have characterized the functional shape of individual structures fitting them with Gaussian and parabolic functions respectively after and before the action of the filter as it is clearly depicted in Supplemental Fig. 7.



Supplemental FIG. 7. In (a) we present a section of the pattern depicted in Supplemental Fig. 5(b), in blue is the intensity profile before filtering while in red after filtering. In (b) and (c) are the fits of the single structures respectively after (Gaussian fit) and before (parabolic fit) the filter action.